J Appl Electrochem (2013) 43:1043–1054
DOI 10.1007/s10800-013-0586-6

RESEARCH ARTICLE

Synthesis, characterization, and electrochemical evaluation of anti-corrosive performance of poly((*N*-methacryloyloxymethyl) benzotriazole-*co*-*N*-vinylpyrrolidone) coatings

K. M. Govindaraju · D. Gopi · K. Anver Basha

Received: 16 February 2013 / Accepted: 13 July 2013 / Published online: 24 July 2013

Abstract Poly((*N*-methacryloyloxymethyl)benzotriazole-*co*-*N*-vinylpyrrolidone) was synthesized by free radical solution polymerization technique and characterized using Fourier transform infrared spectroscopy and nuclear magnetic resonance spectroscopy. Thermal stability of the synthesized copolymer was analyzed by thermogravimetric analysis and differential thermal analysis. The corrosion performances of low nickel stainless steel specimens coated with different mole ratios of synthesized copolymer were investigated in 1 M H_2SO_4 using potentiodynamic polarization, electrochemical impedance method, and chronoamperometric studies. Surface and morphological investigation were also provided in order to characterize the adherence and uniformity of the coatings. Electrochemical corrosion test and surface analysis results were clearly showed that the copolymer-coatings served as a stable host matrix on low nickel stainless steel as environmentally favored good anticorrosive coating.

Keywords Methacrylate polymer · Organic coating · Corrosion · Potentiodynamic polarization · EIS

K. M. Govindaraju (✉)
Department of Chemistry, Mahendra Engineering College, Namakkal 637503, Tamil Nadu, India
e-mail: govindh82@gmail.com

D. Gopi
Department of Chemistry, Periyar University, Salem 636011, Tamil Nadu, India

K. Anver Basha
PG & Research Department of Chemistry, C. Abdul Hakeem College, Melvisharam, Vellore 632509, Tamil Nadu, India

1 Introduction

The modern coating technology is focused to the need of development of high performance polymeric materials [1–3]. These materials are required for coatings with superior mechanical, thermal, and anticorrosive characteristics to overcome the adverse environmental conditions [4].

Hence, novel approaches are sought for by companies to replace such undesired anticorrosive materials. The protection of metals against corrosion through the use of polymeric coatings has been the subject of considerable research in recent years [5–7], particularly in the protection of stainless steel and aluminium alloys [8–11]. The potential of conducting organic polymers for corrosion protection is a topic of current interest [12–14]. However, the efficacy of these materials depends on many factors like how they are applied, the doping level, the conditions of the corrosion experiments, etc. The hydrophilic and porous nature of the conducting polymer films also lead to some serious drawbacks for anticorrosive applications under severe conditions [15–17]. The copolymerization has long been utilized to improve various properties of polymer films [18]. The use of organic polymers, which have been shown to pose corrosion potential of oxidizable metals in passive range, is an attractive option. The protection provided by organic polymers inhibits or delays corrosion of coated metals initiated by the coating defects, which are usually responsible for eventual coating failures. Most of the polymers are potentially permeable to corrosive species, exposure of polymeric coatings to corrosive environments results in swelling, ablation, and variation in resistance of the coating. These in turn change the protection characteristics of the coating system [19].

The growing interests in these organic copolymers are due to their characteristic architectural features, which

offer the end products with enhanced properties as compared to alternative homopolymer systems. Methacrylates, based polymers, are a class of important materials and their wide spread applications drive efforts to prepare materials with improved properties [4, 8, 11]. The advantage of methacrylate-based polymers is their high thermal, chemical, and mechanical stability, which makes them good candidates for applications that require adhesion to various substrates, abrasion resistance, flexibility, toughness, and good resistance to chemicals and water. The degradation temperature of such polymers can be as high as 500 °C. In addition, due to the high molecular weight and mechanical stability of methacrylate-based polymers, low thickness films can be coated on the metallic surface. Hence, it is worthwhile to evaluate the coating performance of methacrylate-based copolymers for their potential application in the corrosion protection of stainless steel. They just form a physical barrier against the attack of corrosive species from the environment and reduce the corrosion and abrasion rate of the substrate. This serves an efficient way to protect metallic substrates from corrosion. The another main advantage of polymeric coatings as compared to chemical inhibitors are the ease of their deposition, low toxicity, and low impact on the environment and human health.

This study is focused to exploit the adhesive and protective behavior of poly(MMBT-*co*-*N*-Vp) by synthesizing different mole ratios of poly((*N*-methacryloyloxymethyl)benzotriazole-*co*-*N*-vinylpyrrolidone) (MMBT) and *N*-vinylpyrrolidone (*N*-Vp). The homogenous and free from pores of copolymer was coated on LN SS through drop casting method to increase the adhesion and protective properties against corrosion. Synthesized poly(MMBT-*co*-*N*-Vp) has been characterized by FT-IR, ^{1}H NMR, ^{13}C NMR, TGA, and DTA techniques. To evaluate the corrosion protection properties of this copolymers, the electrochemical experiments such as potentiodynamic polarization, electrochemical impedance spectroscopic (EIS), and chronoamperometric studies and surface analysis like SEM and EDAX techniques were carried out with LN SS samples coated with different mole ratios of the copolymers in 1 M H_2SO_4.

2 Experimental

2.1 Synthesis of poly((N-methacryloyloxymethyl) benzotriazole-co-N-vinylpyrrolidone)

Initially, *N*-hydroxymethyl benzotriazole was synthesized by Mannich base reaction. In the second stage,

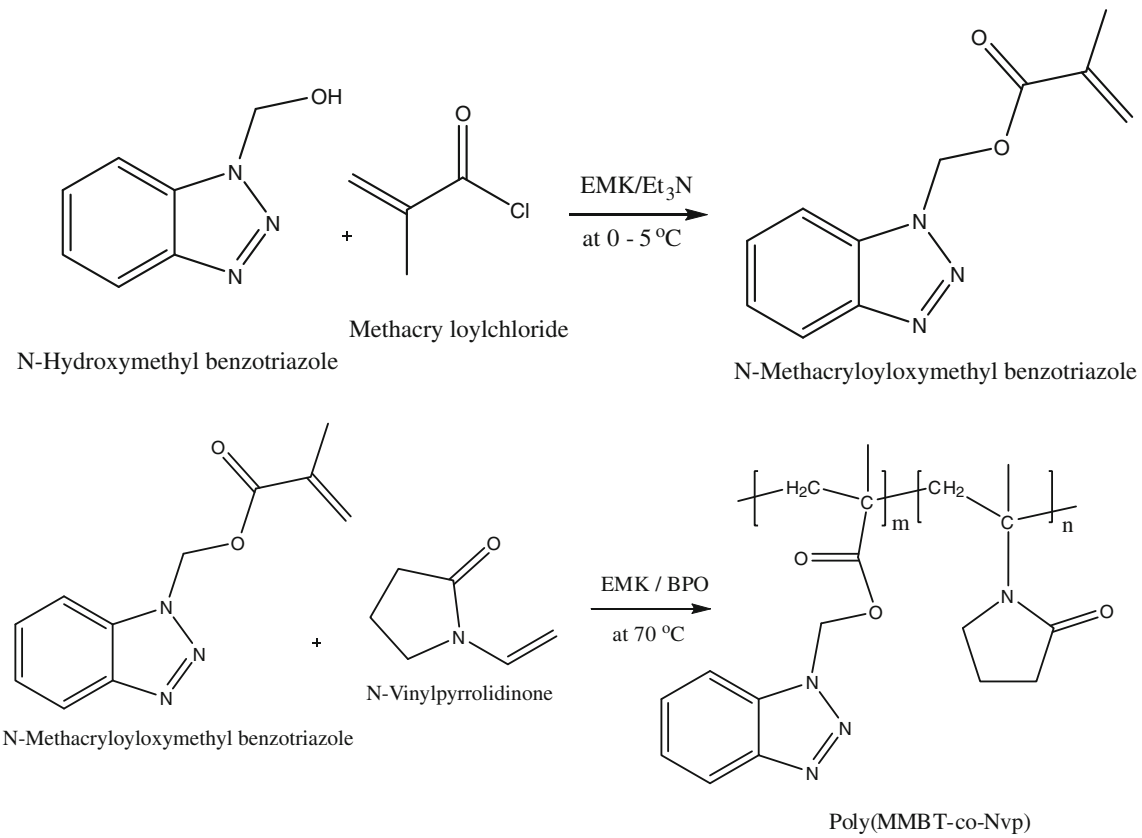

Scheme 1 Synthesis of *N*-methacryloyloxymethyl benzotriazole and poly(*N*-methacryloyloxymethyl benzotriazole-*co*-*N*-vinyl pyrrolidinone)

N-methacryloyloxymethyl benzotriazole (MMBT) was synthesized by reacting *N*-hydroxymethyl benzotriazole (0.022 mol) with methacryloyl chloride (0.022 mol) in ethylmethyl ketone (300 ml) in the presence of triethyl amine (0.022 mol) and maintained in the temperature range 0–10 °C. In the third stage, copolymer poly(MMBT-*co*-*N*-Vp) was synthesized by free radical solution polymerization of the monomers namely *N*-methacryloyloxymethyl benzotriazole (MMBT) and *N*-vinylpyrrolidinone (*N*-Vp). The various mole ratios of MMBT and *N*-Vp namely 0.20:0.80, 0.35:0.65, 0.50:0.50, 0.65:0.35, and 0.80:0.20 were used with BPO as initiator in ethylmethyl ketone solvent. A schematic representation of the synthesis of MMBT and poly(MMBT-*co*-*N*-Vp) are shown in Scheme 1.

2.2 Spectral and thermal characterization of poly(MMBT-*co*-*N*-Vp)

The synthesized copolymers poly(MMBT-*co*-NVp) were characterized by FT-IR spectrophotometer (Model: Perkin-Elmer paragon 1000) in the wave number range of 4,000–400 cm^{-1} using KBr pellets. The structures of synthesized copolymers were further confirmed by ^{1}H and ^{13}C NMR spectroscopic techniques (Model: Jeol GSX-400 MHz) using deuterated chloroform as a solvent. Thermal stability of synthesized copolymers was determined by thermogravimetric analysis (TGA) and differential thermal analysis (DTA) (Model: Mettler TA 3000 thermal analyzer) at a heating rate of 20 °C min^{-1} under dry nitrogen.

2.3 Preparation of specimens

Austenitic low nickel stainless steel, (LN SS) sample was used as material for the corrosion studies. The chemical composition of LN SS was determined by analytical techniques and its composition in wt% is illustrated in the Table 1.

All the test specimens of LN SS were cut into an overall apparent size of 1 × 1 × 0.3 cm and embedded using epoxy resin with an electrical connection and exposed area of 1 cm^2. These specimens were polished with different grits of SiC papers namely 120, 320, 400, 600, 800, 1000, and 1,200 degreased with acetone and finally rinsed with distilled water. The synthesized poly(MMBT-*co*-*N*-Vp) were dissolved in dichloromethane and coated on electrode surface by drop casting technique and dried at room temperature. These coated electrodes were used for the subsequent tests. The reproducibility was checked by repeated measurements (three times).

2.4 Electrochemical studies

2.4.1 Potentiodynamic polarization studies

All the electrochemical measurements were performed using the Electrochemical Workstation (Model No.: CHI 760C, CH Instruments, USA) and a constant temperature of 28 ± 1 °C is maintained with 1 M H_2SO_4 as an electrolyte. A platinum electrode and a saturated calomel electrode (SCE) were used as auxiliary and reference electrodes, respectively, while the working electrode comprised of LN SS specimens of 1 cm^2 exposed area. The tip of the reference electrode was positioned very close to the surface of the working electrode by the use of a fine Luggin capillary in order to minimize the ohmic potential drop. The remaining uncompensated resistance was also minimized by the electrochemical workstation during the scan. Potentiodynamic polarization studies were carried out in the potential range of −1,000 to 1,000 mV for uncoated and copolymer-coated austenitic low nickel stainless steel at a scan rate of 0.1 mV s^{-1}.

2.4.2 Electrochemical impedance studies

The electrochemical impedance studies were carried out using the same setup as that of potentiodynamic polarization studies and the applied ac perturbation signal was about 10 mV within the frequency range of 100 kHz to 1 Hz. The electrochemical impedance measurements were carried out at open circuit potential.

2.4.3 Chronoamperometric measurements

Chronoamperometric measurements were carried out in order to study the progress and stability of the corrosion products in 1 M H_2SO_4 using the same setup as that of potentiodynamic polarization studies by applying a constant potential of 800 mV versus SCE for 1,000 s.

2.4.4 Surface characterization

The morphology and surface elemental composition of the uncoated and copolymer-coated austenitic LN SS were

Table 1 The chemical composition of austenitic low nickel stainless steel

Element	C	Si	Mn	P	S	Cr	Ni	N	Cu	Fe
(wt%)	0.063	0.35	7.05	0.05	0.01	16.03	4.16	0.1	1.24	70.94

investigated using scanning electron microscope (JEOL Model JSM-6390LV) with energy dispersive X-ray analysis (JEOL Model JED-2300).

3 Results and discussion

3.1 FT-IR spectral analysis of poly(MMBT-*co*-*N*-Vp)

The FT-IR spectrum for the copolymer poly(MMBT-*co*-*N*-Vp) was recorded in order to confirm the structure of the copolymer and it is shown in Fig. 1. The peak at 3,093 cm^{-1} could be attributed to aromatic C–H stretching while the C–H stretching due to the methyl and methylene groups were observed at 2,994 and 2,950 cm^{-1}. The carbonyl stretching, due to the ester group, was detected at 1,733 cm^{-1}. The C=O stretching vibration, due to the amide and NVp, has appeared at 1,668 cm^{-1}, and the aromatic C=C stretching were observed at 1,500 and 1,452 cm^{-1}. The signal, due to N=N stretching, overlapped with that of C=C stretching and was found at 1,452 cm^{-1}. The C–N stretching detected at 1,380 cm^{-1}. The peaks observed at 1,263 and 1,147 cm^{-1} could be attributed to C–O stretching and the C–H out of plane bending vibration of the aromatic ring was observed at 752 cm^{-1}. The peak at 659 cm^{-1} was due to the C–C out of plane bending vibration of the aromatic ring.

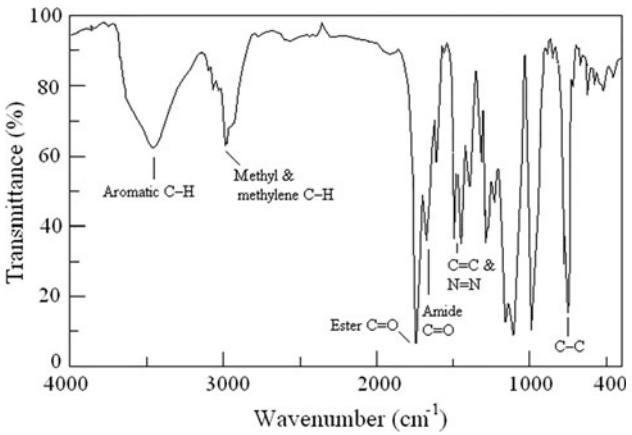

Fig. 1 FT-IR spectrum of poly(MMBT-*co*-NVp)

3.2 NMR spectral analysis of poly(MMBT-*co*-*N*-Vp)

The ^{1}H NMR spectrum of the copolymer poly(MMBT-*co*-*N*-Vp) is shown in Fig. 2. The NMR spectrum is very broad and overlapped. All the chemical shift assignments for the synthesized copolymers were based on the chemical shifts observed for the respective monomers and homopolymers. The aromatic protons show signals between 8.16 and 7.32 ppm. The signal at 5.91 and 5.63 ppm is due to the methylenoxy group in MMBT units. The methylene group of the copolymer backbone shows a broad signal between 2.5 and 2.1 ppm due to tacticity. A sharp peak at 1.6 ppm corresponds to the methyl protons. The back bone protons of MMBT overlapped with the back bone protons of *N*-Vp. Thus participation of two monomeric units in the copolymer was confirmed.

The complete assignment of the proton decoupled ^{13}C NMR spectrum of the copolymer poly(MMBT-*co*-*N*-Vp) in $CDCl_3$ is presented in Fig. 3. The carbonyl >C=O carbon signals for *N*-vinylpyrrolidine resonate around 169.9–172.65 ppm. The resonance signals at 174.98 ppm was due to the carbonyl carbon directly attached to the polymer back bone. The resonance signals observed at 131.42–122.09 ppm was due to the aromatic carbons. The structural

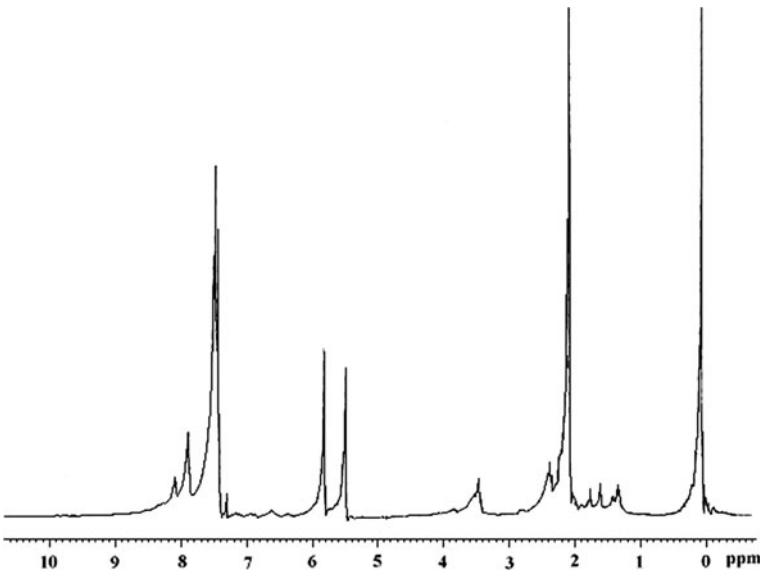

Fig. 2 ^{1}H NMR spectrum of poly(MMBT-*co*-NVp)

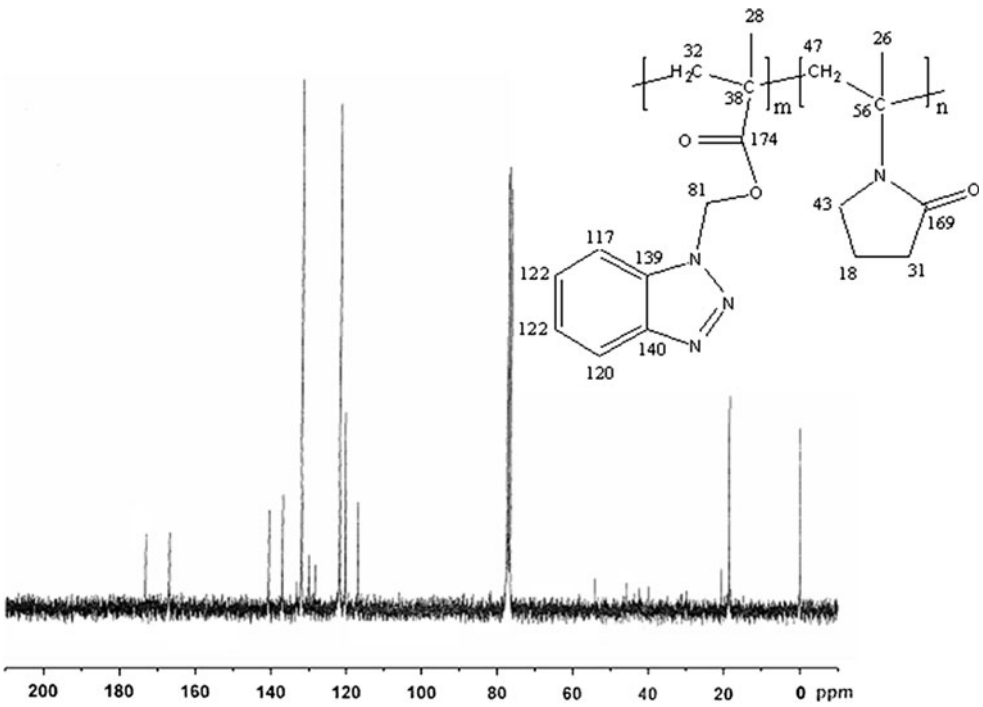

Fig. 3 ^{13}C NMR spectrum of poly(MMBT-*co*-NVp)

region around 54–15 ppm is quite complex, which can be assigned to aliphatic carbon (methylene and tertiary carbons) resonances in the main backbone as well as the side chain of the poly(MMBT-*co*-*N*-Vp) copolymer. The α-methyl group of both monomeric units shows a series of resonance signals between 18.25 and 19.93 ppm due to tacticity.

3.3 Thermal analysis of poly(MMBT-*co*-*N*-Vp)

The thermogravimetric curve for poly(MMBT-*co*-*N*-Vp) is shown in Fig. 4. Poly(MMBT-*co*-*N*-Vp) has also demonstrated a considerable thermal stability as evident from the thermogram. The initial decomposition temperature (IDT) was detected around 160 °C, and the initial decomposition rate was observed to be low up to a temperature range of 160–260 °C. At temperatures above 260 °C, poly(MMBT-*co*-*N*-Vp) showed one main stage of degradation. The first stage weight loss (53 %), starting particularly from 160 to 345 °C, corresponds to the cleaving of the bulky azole and amide groups. The thermogravimetric curves of poly (MMBT-*co*-*N*-Vp) suggested that the effective degradation of the copolymers occurred at first and second stage in the temperature range between 160 and 425 °C. At this stage, the percentage of mass loss was in the range of 75–83 %. Thus, the rapid decomposition detected in this stage may be the cause of the cleavage of the azole group, followed by the elimination of the resultant low molecular weight fragments.

The composition of the constitutional monomeric units in the copolymer decides the actual decomposition temperature range observed for the polymer. The initial decomposition temperature decreases a little with the increase of MMBT content in the copolymer. The thermal stability of these copolymers were found good with the increase of *N*-Vp content in the copolymer chain. The percentage weight loss and the degradation temperature of poly(MMBT-*co*-*N*-Vp) synthesized from 0.35:0.65, 0.50:0.50, and 0.65:0.35 mol ratios are given in Table 2.

The DTA curve obtained for the poly(MMBT-*co*-*N*-Vp) copolymer is presented in Fig. 5. It was observed that each sample exhibits similar thermal degradation behavior and the overall variation in thermal stability also appears to be small which could be attributed to their identical decomposition values obtained through the thermogram.

3.4 Solubility test

The solubility of the synthesized copolymer derivatives were tested in various solvents in room temperature. All studied copolymers were easily soluble in various organic solvents namely, acetone, dichloromethane, toluene, benzene, 1,4-dioxane, chloroform, and chlorobenzene. But these polymers are partially soluble in dimethyl formamide and insoluble in water, methanol, and ethanol. The solubility test results are presented on Table 3 and it clearly shows that there is wide possibility for using different solvents for the copolymers in order to be used in coating applications.

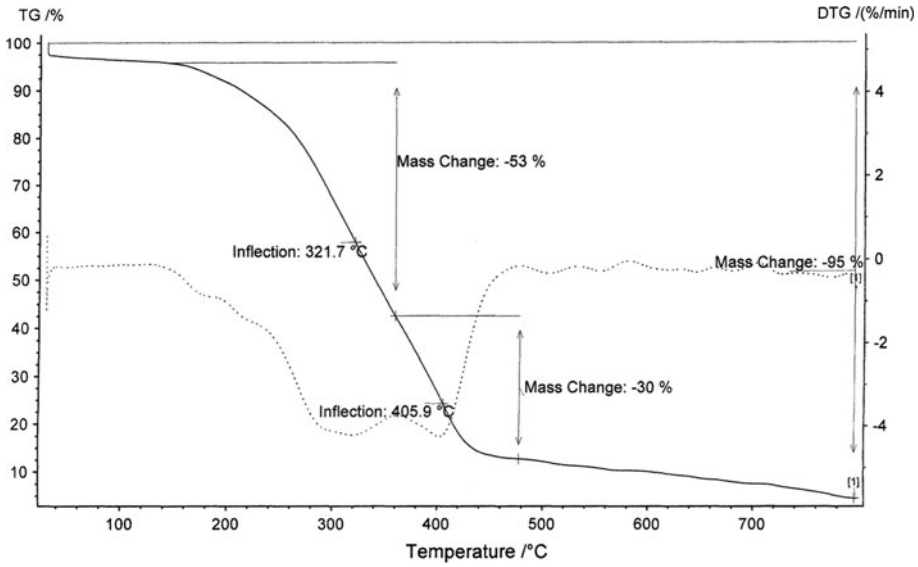

Fig. 4 TGA of poly(MMBT-*co*-NVp)

Table 2 Thermogravimetric data of poly(MMBT-*co*-NVp)

Poly(MMBT-*co*-NVp)	IDT (°C)	Temperature (°C) at weight loss (%)				
		10 %	30 %	50 %	70 %	90 %
35:65	160	221	235	248	342	488
50:50	176	230	244	259	349	520
65:35	184	243	260	273	326	512

3.5 Potentiodynamic polarization studies

The potentiodynamic polarization curves of uncoated and different mole ratio of poly(MMBT-*co*-*N*Vp)-coated austenitic LN SS in 1 M H_2SO_4 is shown in the Fig. 6. For all the poly(MMBT-*co*-*N*-Vp)-coated LN SS shows reduced current density in both cathodic and anodic region than that of the uncoated low nickel stainless steel. The corrosion potential was displaced towards positive values for 0.35:0.65 and 0.50:0.50 mol ratios of poly (MMBT-*co*-*N*-Vp)-coated LN SS and this could be attributed to the formation of coatings with poor protective properties. Besides this, the dissolution reaction appeared to be a little more polarized at low over-potentials. As can be seen from the Fig. 6, though all the samples shows considerable decrease in the corrosion current density, a very low value was observed for the sample coated with 0.65:0.35 mol ratio of poly(MMBT-*co*-*N*-Vp). The corrosion current density of LN SS coated with 0.65:0.35 mol ratio of poly(MMBT-*co*-*N*-Vp) was found to be 0.944×10^{-4} A and it increased significantly by coating the alloy with increasing of *N*-Vp ratio.

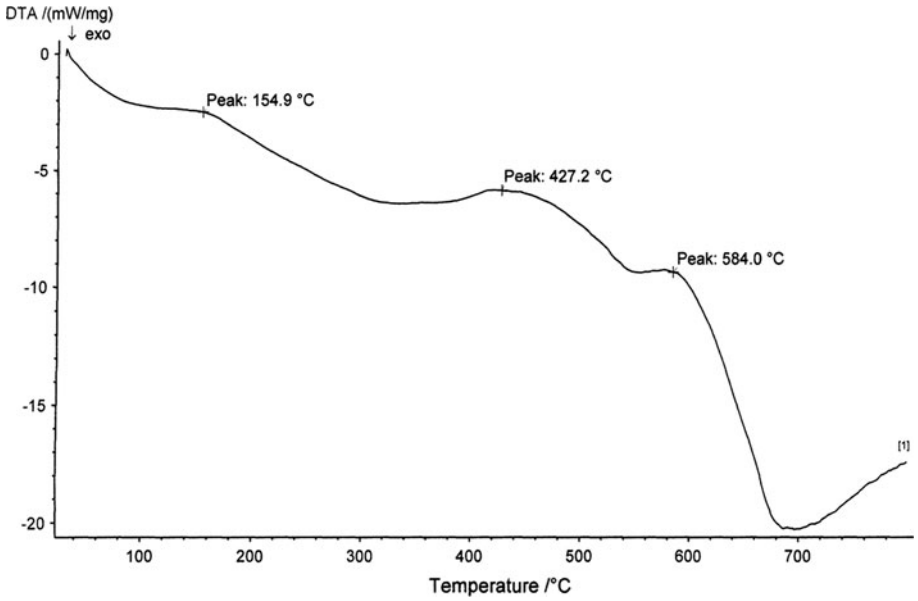

Fig. 5 DTA of poly(MMBT-*co*-NVp)

Table 3 Solubility behavior of poly(MMBT-*co*-NVp)

Polymer composition	Solubility in various solvents						
	Acetone	Dichloromethane	Toluene	Benzene	Chloro-form	Dimethyl formamide	Water, methanol & ethanol
0.20:0.80	++	++	++	++	++	+	–
0.35:0.65	++	++	++	++	++	+	–
0.50:0.50	++	++	++	++	++	+	–
0.65:0.35	++	++	++	++	++	+	–
0.80:0.20	++	++	++	++	++	+	–

'++' completely soluble; '+' partially soluble; '–' insoluble even on heating

Hence, the LN SS coated with 0.65:0.35 mol ratio of poly(MMBT-*co*-*N*-Vp), showed good protection than the sample coated with other mole ratios of this copolymer. Hence, it is suggested that the copolymer poly(MMBT-*co*-*N*-Vp) coated on LN SS also restricts the interaction between the alloy and the electrolyte. The potentiodynamic polarization parameters of every individual ratio of the copolymer poly(MMBT-*co*-*N*-Vp) is presented in Table 4. From this table, the E_{corr} of LN SS coated with poly(MMBT-*co*-*N*-Vp) shows a shift on both active and noble direction.

3.6 Electrochemical impedance studies

Electrochemical impedance spectroscopy (EIS) is a well established quantitative method for examining the anti-corrosion performance of the organic coating [20, 21]. The result of EIS is the impedance of the electrochemical system as a function of frequency. The response of the electrochemical system to small voltage perturbations of various frequencies can give useful information about the properties of the protective-coating system [22]. Usually impedance is described with an equivalent electrical circuit constructed preferably by circuit elements with proper electrochemical background [23]. Evaluations of protective coatings are often combinations of EIS spectra measurements, immersion in electrolyte solution, or various accelerated exposures [24, 25].

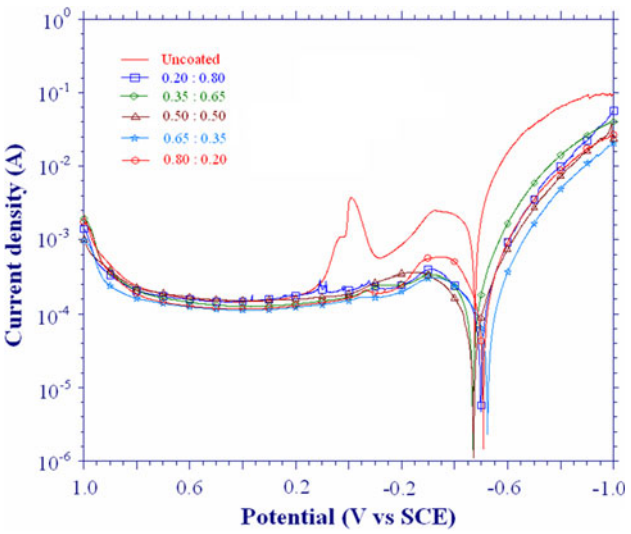

Fig. 6 Potentiodynamic polarization *curves* for uncoated and poly(MMBT-*co*-NVp) coated low nickel stainless steel in 1 M H_2SO_4

The protective effect of all the studied methacrylate-based copolymer coating is evaluated using the electrochemical impedance spectroscopy (EIS). An equivalent circuit such as given in Fig. 7a, was used to consider all the process involved in the electrical response of the system. The first element in the circuit is a solution resistance (R_s), which corresponds to the ohmic resistance of the system. The C_{dl} represents the double layer capacitance, and a resistance R_1 represents the resistance to the charge transfer of the oxidation of the alloy. The second subsystem corresponds to the resistance (R_2), and the capacitance of the coating which is a passive film in the case of uncoated austenitic low nickel stainless steel. The different elements were evaluated by a fitting procedure.

In the case of uncoated LN SS in 1 M H_2SO_4 environment, the equivalent circuit such as shown in Fig. 7b, was used to consider the electrical response of the system. The first resistance (R_1) corresponds to the oxidation of the metal after this oxidation iron and chromium oxides film is formed. This film has a higher resistance due to passive characteristics. The capacity constant phase element (CPE) of this film was simulated as a constant phase element too. This was often attributed to roughness and inhomogeneities of the solid surface in aggressive environment [26]. Hence, a CPE is used instead of a capacitive element to get a more accurate fit of experimental data sets using generally more complicated equivalent circuits.

The anti-corrosive behavior of copolymer poly(MMBT-*co*-*N*-Vp) coatings on LN SS in 1 M H_2SO_4 solution was investigated using EIS technique. The Nyquist plots for uncoated LN SS and coated with various compositions, namely 0.20:0.80, 0.35:0.65, 0.50:0.50, 0.65:0.35, and 0.80:0.20 mol ratio of poly(MMBT-*co*-*N*-Vp) are presented

Table 4 Potentiodynamic polarization parameters obtained for various mole ratios of poly(MMBT-*co*-NVp) coated and uncoated low nickel stainless steel in 1 M H_2SO_4

Sample	E_{corr} (mV)	β_a (V/dec)	β_c (V/dec)	i_{corr} (10^{-4} A cm^{-2})	E_b (mV)	Rate (mpy)
Uncoated	−476	0.24	6.82	41.16	758	185.9
0.20:0.80	−508	4.11	7.82	2.104	834	9.50
0.35:0.65	−469	2.74	8.05	1.923	904	8.68
0.50:0.50	−472	4.51	7.78	1.193	908	5.38
0.65:0.35	−525	3.22	7.73	0.944	937	4.26
0.80:0.20	−499	2.67	8.13	1.923	854	8.68

Fig. 7 The equivalent circuit

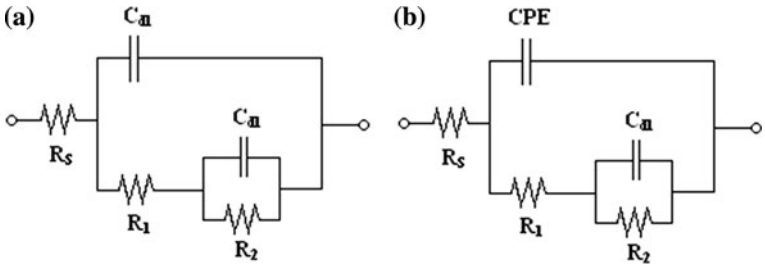

in Fig. 8. In the presence of all the studied composition of copolymer the austenitic LN SS exhibit high resistance against corrosion. The diameter of the semicircle has increased with respect to the composition of the poly(MMBT-*co*-*N*-Vp) and a maximum value for 0.65:0.35 mol ratio of this copolymer. The resistance increases as a consequence of the presence of the poly(MMBT-*co*-*N*-Vp) film which avoids the penetration of the electrolyte. The capacitance of all the coated specimen is lower than the uncoated LN SS specimen, due to the copolymer film over the substrate which reduces the amount of electrolyte in contact with the alloy.

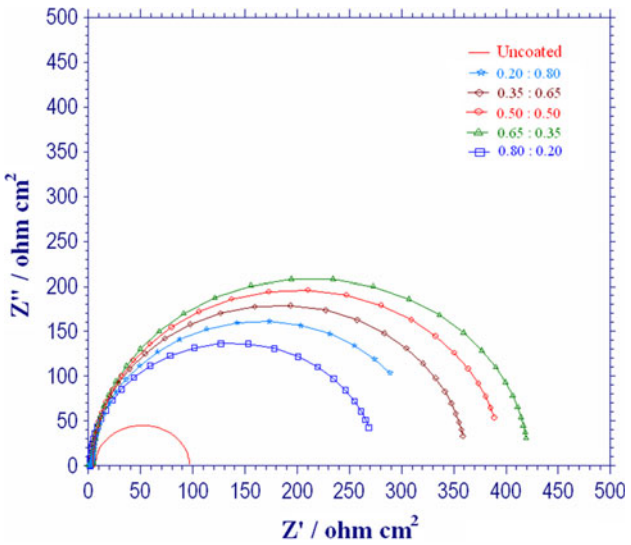

Fig. 8 Nyquist plots for uncoated and various mole ratios of poly(MMBT-*co*-NVp) coated LN SS in 1 M H_2SO_4

The semicircular region was attributed to the sum of charge transfer resistance against LN SS dissolution and the polymer film resistance. The lowest and highest mole ratio of poly(MMBT-*co*-*N*-Vp)-coated LN SS shows minimum R_{ct} value and maximum C_{dl}. This high value of R_{ct} is due to little penetration of corrosive ions on copolymer coating. As the *N*-Vp composition increases the adhesiveness of the poly(MMBT-*co*-*N*-Vp) on LN SS decreases, and this in turn decrease the anti-corrosive performance.

The linear portion was related to the resistance against diffusion of corrosive species through the pores of the copolymer film. The impedance parameters derived from the Nyquist plots for uncoated and copolymer poly(MMBT-*co*-*N*-Vp)-coated LN SS in 1 M H_2SO_4 are given in Table 5. As can be seen from the Table 5, the high R_{ct} value of copolymer coated LN SS suggested a good corrosion protection efficiency of these copolymers. However, the poly(MMBT-*co*-*N*-Vp) synthesized from 0.65:0.35 mol ratio of MMBT and NVp showed lower C_{dl} and higher R_{ct} values compared to the copolymer synthesized from other mole ratios which might be due to the good adhesive and protective behavior of MMBT and NVp. The decrease in C_{dl} value, resulting from a decrease in local dielectric constant and increase in the strength of the double layer, suggested that the poly(MMBT-*co*-*N*-Vp) molecules function by strong adhesion on the LN SS surface.

The Bode plots for the uncoated and copolymer poly(MMBT-*co*-*N*-Vp) coated LN SS in 1 M H_2SO_4 are shown in Fig. 9a, b. The low frequency data in Bode plots has usually been associated with the diffusion processes [27]. As it is known the diameter of EIS curve can be equal to the charge transfer resistance value of the alloy electrode [28]. Furthermore, the diameter of the semicircles

Table 5 Electrochemical impedance parameters obtained for uncoated and various mole ratios of poly(MMBT-*co*-NVp) coated LN SS in 1 M H_2SO_4

Sample	R_{ct} (Ω)	C_{dl} (μF cm^{-2})
Uncoated	90.26	0.553
0.20:0.80	296.9	0.311
0.35:0.65	312.4	0.270
0.50:0.50	395.1	0.234
0.65:0.35	423.4	0.198
0.80:0.20	270.9	0.326

decreases as the mole ratios differ. Thus the charge transfer resistance of the coating decreases with composition, and accounts for coating degradation. It is evident that the poly(MMBT-*co*-*N*-Vp)-coated specimens showed an increase in the maximal phase angle value which indicates a good barrier effect of this copolymer.

3.7 Chronoamperometry studies

Figure 10 shows the chronoamperometric curves of uncoated and different mole ratios of poly(MMBT-*co*-*N*-Vp)-coated LN SS in 1 M H_2SO_4. As evident from the figure, the copolymer synthesized from all the mole ratio of poly(MMBT-*co*-*N*-Vp)-coated LN SS shows a constant negative current with a steady value of around −0.1 to −0.2 mA. In the case of copolymer poly(MMBT-*co*-*N*-Vp) synthesized from 0.65:0.35 mol ratio show the steady current value around −0.2 mA.

Poly(MMBT-*co*-*N*-Vp) synthesized from high mole ratio of MMBT have showed some fluctuations in the entire duration, which is due to the dissolution and the backing of the protective polymer layer. Apparently, this copolymer poly(MMBT-*co*-*N*-Vp) coating except 0.20:0.80 mol ratio exhibits considerable protection against the dissolution of LN SS. The poor performance of the copolymer 0.20:0.80 mol ratio may occur due to the poor adherence and brittleness of the coating.

3.8 Surface characterization

3.8.1 SEM and EDAX analysis

The SEM image of the uncoated LN SS after potentiodynamic polarization test is shown in Fig. 11a. The micrograph shows numerous pits on the surface which indicates the deterioration of the LN SS substrate. Since there is no protection on the surface of the substrate, the effect of corrosive ions present in the electrolyte is evidenced on the surface of LN SS. The EDAX pattern obtained also substantiates this fact since peaks corresponding to Fe and Cr are evident from the EDAX pattern (Fig. 11b).

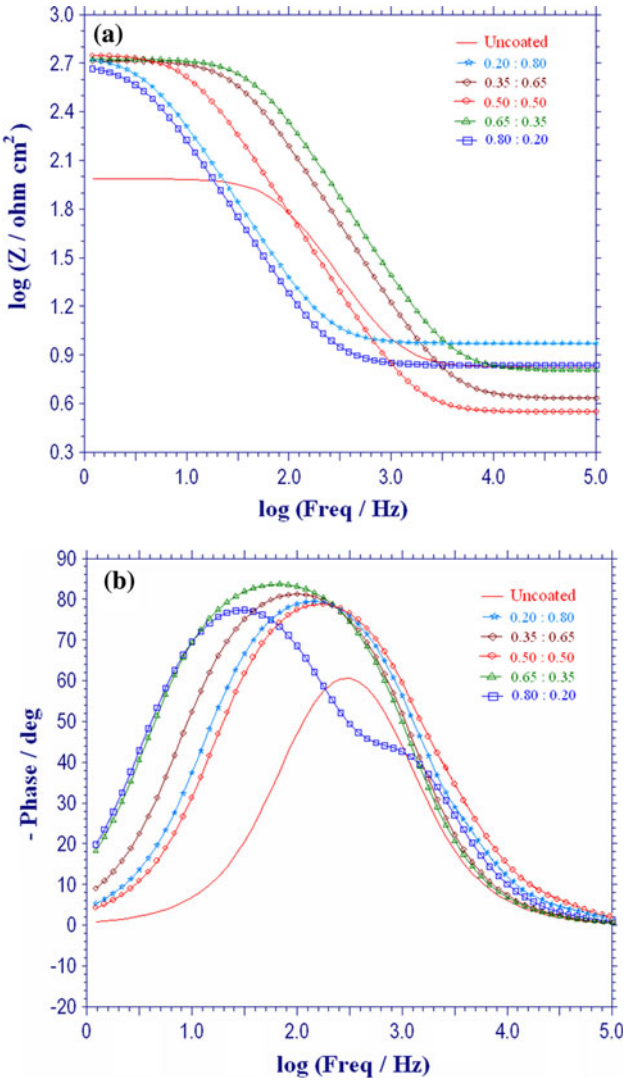

Fig. 9 Bode plots for uncoated and various mole ratios of poly(MMBT-*co*-NVp) coated LN SS in 1 M H_2SO_4

The SEM image of poly((*N*-methacryloyloxymethyl)benzotriazole-*co*-*N*-vinylpyrrolidone) film developed on austenitic LN SS is presented in Fig. 12a. It is evident from the micrograph that a layer of copolymer covers the entire surface of the LN SS which prevents its deterioration in the corrosive solution. As a result, pits are seldom seen on the surface, and no detachment of polymer coverage is noted. The elemental composition of the polymer formed over the LN SS substrate which was detected by EDAX pattern is shown in Fig. 12b. The obtained pattern indicates that the composition of the film formed over the substrate surface is identical to the parent compound, thus confirming the formation of the copolymer film over the LNSS surface.

Figure 13a shows the SEM image of poly(MMBT-*co*-*N*-Vp) coated austenitic LN SS after the potentiodynamic polarization test and its corresponding EDAX pattern is presented in Fig. 13b. From the SEM image it is noted that,

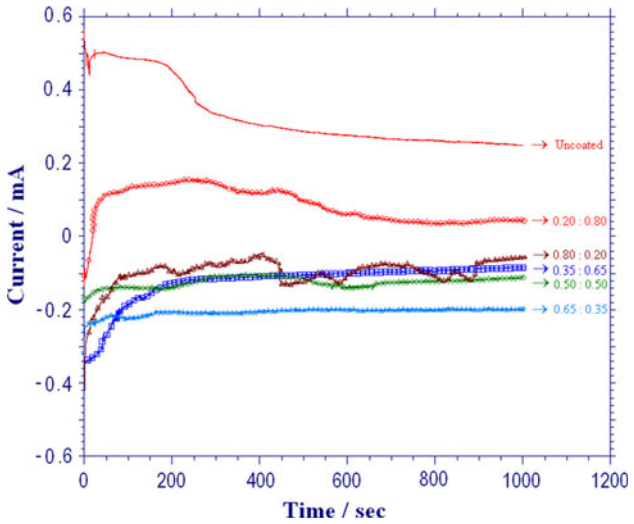

Fig. 10 Chronoamperometric curves for uncoated and various mole ratio of poly(MMBT-*co*-NVp) coated LN SS in 1 M H_2SO_4

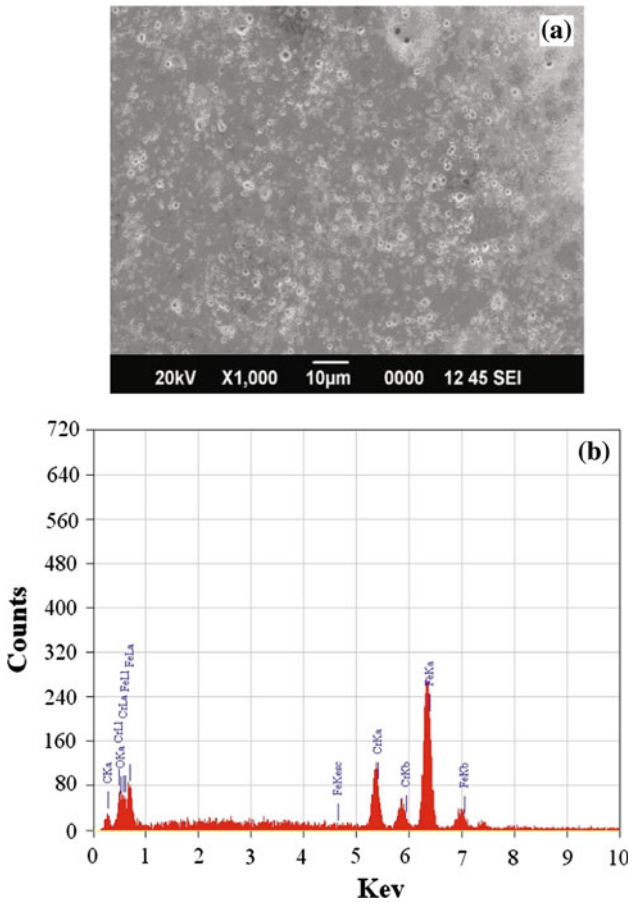

Fig. 11 **a** SEM and **b** EDAX pattern of uncoated austenitic LN SS after potentiodynamic polarization test in 1 M H_2SO_4

the polymer tends to form a uniform coverage of protective layer over the LN SS surface. However, a slight deterioration in the film has occurred during the exposure to the corrosive electrolyte which is evident from the micrograph. This may be due to the less adherent nature of the polymer, because of which a portion of the coating could have peeled off from the substrate. However, no considerable substrate deterioration is observed thus confirming the corrosion protection offered by the copolymer.

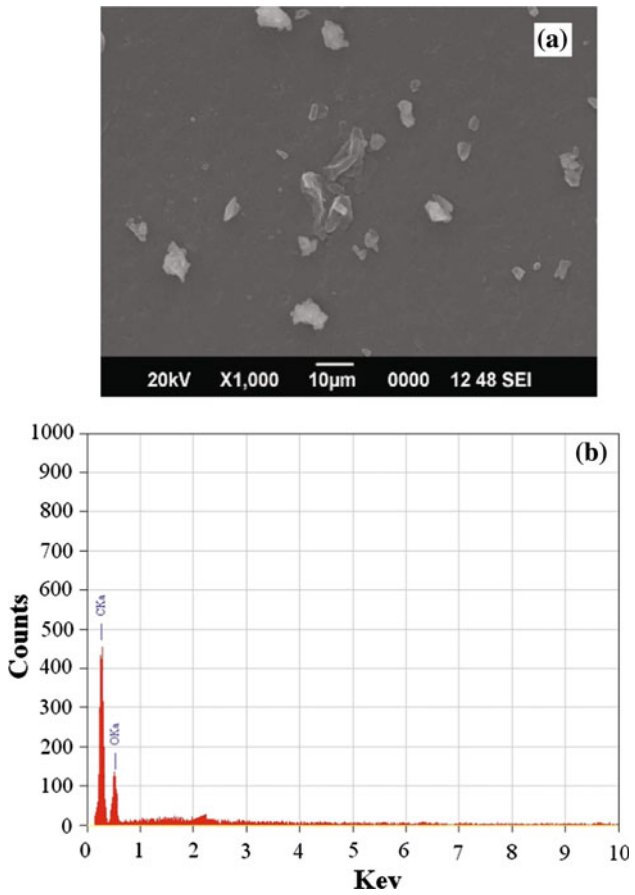

Fig. 12 **a** SEM and **b** EDAX pattern of poly(MMBT-*co*-NVp) coated austenitic LN SS

The EDAX pattern of the polymer also confirms that the coverage is uniform over the LN SS surface and the composition obtained for the coating is also an agreement with the composition of the polymer. The EDAX pattern of poly(MMBT-*co*-*N*-Vp)-coated LN SS after potentiodynamic polarization test exhibit considerable amount of Fe and traces of Cr which could be due to some deterioration of the poly(MMBT-*co*-*N*-Vp)-coated LN SS substrate in the electrolyte.

3.9 Mechanism for corrosion protection

The possible mechanism for the performance of the copolymers, as anti-corrosive agents on low nickel stainless steel, depends on their structure and type of monomer unit. The increase in the corrosion protection efficiency of

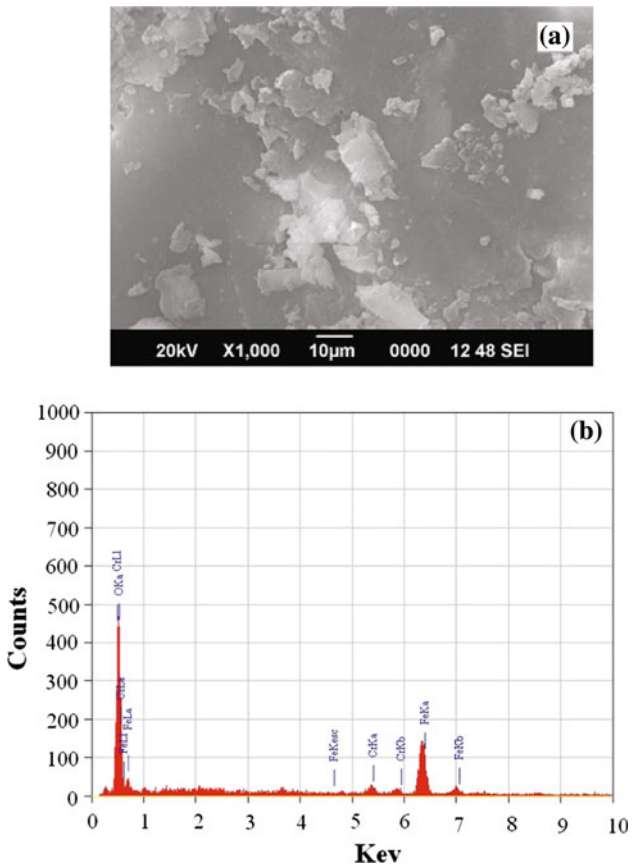

Fig. 13 **a** SEM and **b** EDAX pattern of poly(MMBT-*co*-NVp) coated austenitic LN SS after potentiodynamic polarization test in 1 M H_2SO_4

these methacrylate-based copolymer coatings on the alloy surface may have probably resulted from the better adhesion of the copolymers coating on LN SS. The good adherence of the copolymer film to the metal surface in turn depends on the nature of the functional groups, electron-donating heteroatoms and also on the composition and sequence of the monomer units in the copolymers.

In general, the acrylic derivatives have good adhesive nature. The increase in adhesion strength of the methacrylate-based copolymer coatings on LN SS may also be attributed to the existence of good polar attraction between the loan pair electrons on the hetero atom of the copolymer and the LN SS substrate at the coating/substrate interface. The overall corrosion protection offered by the polymer coatings can be attributed to two important factors. The first one is the inhibitive effect, and another one is the barrier effect [29]. The inhibitive effect is observed as a result of interaction of electron-donating atoms, with the metal ions found on the surface of the substrate. As a result of this electrostatic attraction exerted by the electron donating atoms tend to reduce rate of corrosion occurring on the substrate surface.

The barrier effect is much pronounced when an adherent layer of polymer is formed over the substrate surface. This is evident in the studied copolymer systems wherein the composition of combining monomers contributes to the stability and resistivity of the coatings. For instance, the increase in MMBT and decrease in *N*-Vp concentration tend to increase the inhibitive effect up to 0.65:0.35 mol ratio and then the further increase in MMBT concentration leads to the reduction in adhesion behavior of the copolymer film. Copolymer with 0.65:0.35 mol ratio behave as a good adhesive compare to other ratio, due to this adhesion it predominantly control the cathodic reaction and shift the corrosion potential to cathodic side. A parallel explanation could be that, at high composition of MMBT in the copolymer, many of the MMBT units would have another bulky MMBT unit as a neighbour. Due to steric factor, a one of the bulky unit could get attached directly to the metal surface while another unit which is directed to the opposite side (due to tacticity) cannot do so. This would explain the reduced efficiency of corrosion inhibition of 0.80:0.20 mol ratio.

4 Conclusions

1. Novel methacrylate-based anti-corrosive copolymer derivative poly(MMBT-*co*-*N*-Vp) has been successfully synthesized by free radical solution copolymerization method.
2. The stability in 1 M H_2SO_4 medium conditions, and the corrosion resistance of the poly(MMBT-*co*-*N*-Vp) coating were tested, which demonstrated that it has provided an effective way to fabricate a good anticorrosive coating with anticorrosive property in aggressive conditions. All studied mole ratios of this copolymers coating exhibit a mixed type of corrosion protection.
3. The results obtained from three different independent electrochemical techniques like potentiodynamic polarization, electrochemical impedance, and chronoamperometry are in good agreement with each other, and are found to be complementary.
4. Morphological investigation and EDAX analysis have also proved the uniform and good adherent coating.
5. Poly(MMBT-*co*-*N*-Vp)-based organic copolymer coating, among various advantageous properties for industrial application, exhibits high protective effect because of a good corrosion resistance. Therefore, it becomes an extremely high barrier property. This may allow a potential application as anti-corrosive agent for many industrial applications.

Acknowledgments The Financial support by Jawaharlal Nehru Memorial Fund (JNMF), New Delhi, India, and Steel Authority of India Ltd. (SAIL), Salem, Tamil Nadu, India for stainless steel supply, are greatly acknowledged.

References

1. Deligoz H, Yalcinyuva T, Ozgumus S (2005) Eur Polym J 41:771
2. Sharmin E, Imo L, Ashraf SM, Ahmad S (2004) Prog Org Coat 50:47
3. Ashok Kumar A, Alagar M, Rao RMVGK (2001) J Appl Polym Sci 81:38
4. Motheo AJ, Pantoja MF, Venancio EC (2004) Solid State Ion 171:91
5. Herrasti P, Recio FJ, Ocon P (2005) Prog Org Coat 54:285
6. Grundmeier G, Schmidt W, Stratmann M (2000) Electrochim Acta 45:2515
7. Seegmiller JC, da Pereira Silva JE, Torresi RM (2004) J Electrochem Soc 152:644
8. Gopi D, Govindaraju KM, Kavitha L, Anver Basha K (2011) Prog Org Coat 71:11
9. Srikanth AP, Sunitha TG, Raman V, Nanjundan S, Rajendran N (2007) Mater Chem Phys 103:241
10. Roche V, Vacandio F, Bertin D, Gigmes D, Eyraud M (2008) C R Chim 11:1055
11. Bressy C, Margaillan A (2009) Prog Org Coat 66:400
12. Czech Z, Pełech R (2009) Prog Org Coat 65:84
13. Niknahad M, Moradian S, Mirabedini SM (2010) Corros Sci 52:1948
14. Rohwerder M, Michalik A (2007) Electrochim Acta 53:1300
15. Ghosh S, Krishnamurti N (2000) Eur Polym J 36:2125
16. Guilherme MR, Reis AV, Takahashi SH, Rubira AF, Feitosa JPA, Muniz EC (2005) Carbohydr Polym 61:464
17. Monnereau C, Blart E, Montembault Fontaine VL, Odobel F (2005) Tetrahedron 61:10113
18. Luo J, Cheng J, Dong X, Liu Y, Huang G, Zhang J (2010) Appl Surf Sci 256:7389
19. Le Thu Q, Takenouti H, Touzain S (2006) Electrochim Acta 51:2491
20. Kendig M, Scully J (1990) Corrosion 46:22
21. Mansfeld F (1995) J Appl Electrochem 25:187
22. Macdonald DD (1991) Techniques for characterization of electrodes and electrochemical processes. Wiley, New York
23. Skale S, Dolecek V, Slemnik M (2007) Corros Sci 49:1045
24. Deflorian F, Fedrizzi L, Rossi S (1998) Corrosion 54:598
25. Wei DF, Chatterjee I, Jones DA (1995) Corrosion 51:97
26. Rammelt U, Reinhard G (1987) Corros Sci 27:373
27. Hinderliter BR, Croll SG, Tallman DE, Su Q, Bierwangen GP (2006) Electrochim Acta 51:4505
28. Hur E, Bereket G, Sahin Y (2006) Prog Org Coat 57:149
29. Soer WJ, Ming W, Koning CE, van Benthem RATM, Mol JMC, Terryn H (2009) Prog Org Coat 65:94